Inorg. Chem. **2002**, *41*, 1162–1169

Photophysical Effect of the Coordination of Water by Ruthenium(II) Bipyridyl Complexes Containing Hemilabile Phosphine–Ether Ligands

Cerrie W. Rogers,[†] Yan Zhang,[‡] Brian O. Patrick,[†] Wayne E. Jones, Jr.,*[,‡] and Michael O. Wolf*[,†]

Department of Chemistry, University of British Columbia, Vancouver, Canada V6T 1Z1, and Chemistry Department and Institute for Materials Research, State University of New York at Binghamton, Binghamton, New York 13902

Received August 2, 2001

A substantial concentration-dependent red shift of the absorption and emission spectra (77 K) of $[Ru(bpy)_2(POMe\text{-}P,O)]^{2+}$ (**1**) (POMe = (2-methoxyphenyl)diphenylphosphine) is reported. NMR experiments show this shift to be due to equilibration of **1** with an aquo complex (**1b**) ($K_{eff} = (6 \pm 3) \times 10^{-3}$) that forms upon displacement of the coordinated ether in the hemilabile POMe ligand. The excited-state lifetimes of **1** and **1b** at 77 K in solid 2:1 ethanol/acetone solution are $\tau = 2.13 \pm 0.02$ and 1.95 ± 0.02 μs, respectively. The preparation and X-ray crystal structure of a related complex, $[Ru(bpy)_2(PO^iPr\text{-}P)(OH_2)](PF_6)_2$ (**2b**) ($PO^iPr\text{-}P$ = (2-(2-propoxy)phenyl)diphenylphosphine), is also reported. In solution, this species exists as an equilibrium mixture of complexes that cannot be readily separated. This species also has concentration-dependent absorption spectra in 2:1 ethanol/acetone solution, with a significant red shift (20 nm) at lower concentrations.

Introduction

Humidity sensors are technologically important devices due to the need for them in a wide range of applications including the automotive and food industries as well as agriculture.[1,2] A number of different humidity sensors have been developed, with response typically based on capacitance or impedance changes in polymer films or porous ceramics. The materials these devices are based on exhibit many of the desired characteristics (such as stability, sensitivity, and selectivity); however, these technologies tend to suffer from deficiencies related to response time, contamination, and operating temperature. It is therefore of interest to explore new approaches to materials which may be of use in humidity sensing. One possibility is to harness the ability of transition metals to bind Lewis bases such as water. Conveniently, changes in a metal's coordination sphere usually trigger a change in the properties of the metal complex. If the transition-metal framework incorporates a luminophore, the water-binding event can perturb the energetics of the excited state and lead to altered photophysical properties such as luminescence wavelength, intensity, and excited-state lifetime.

Transition-metal complexes with metal-to-ligand charge-transfer (MLCT) excited states are excellent candidates for luminescent sensor applications because of their long-lived luminescence and propensity toward both electron- and energy-transfer quenching processes.[3,4] Several examples of sensors based on these chromophores exist in the literature,[5,6] and most involve coordination of analyte to a receptor site built into the ligand framework. Strategies used include analyte-induced variations in dynamic quenching of the emission intensity and/or lifetime[7,8] and changes in the lowest-energy emitting state.[9] Alternatively, the bipyridyl ligand itself has been used as a binding site for transition metals to create a change in luminescence properties.[10] In the present work we exploit the fact that the nonchromophoric ancillary ligands (L) in $[Ru(bpy)_2L_2]^{2+}$ complexes

* To whom correspondence should be addressed. E-mail: (M.O.W.) mwolf@chem.ubc.ca; (W.E.J.) wjones@binghamton.edu.
[†] University of British Columbia.
[‡] State University of New York at Binghamton.

(1) Kulwicki, B. M. *J. Am. Ceram. Soc.* **1991**, *74*, 697−798.
(2) Yamazoe, N.; Shimuzu, Y. *Sens. Actuators* **1986**, *10*, 379−398.
(3) Kalyanasundaram, K. *Photochemistry of Polypyridine and Porphyrin Complexes*; Academic Press: London, 1992.
(4) Roundhill, D. M. *Photochemistry and Photophysics of Metal Complexes*; Plenum Press: New York, 1994.
(5) de Silva, A. P.; Fox, D. B.; Huxley, A. J. M.; McClenaghan, N. D.; Roiron, J. *Coord. Chem. Rev.* **1999**, *185*, 297−306.
(6) Keefe, M. H.; Benkstein, K. D.; Hupp, J. T. *Coord. Chem. Rev.* **2000**, *205*, 201−228.
(7) Krause, C.; Werner, T.; Huber, C.; Klimant, I.; Wolfbeis, O. S. *Anal. Chem.* **1998**, *70*, 3983−3985.
(8) Oldham, P. B.; McCarroll, M. E.; McGown, L. B.; Warner, I. M. *Anal. Chem.* **2000**, *72*, 197−209.
(9) MacQueen, D. B.; Schanze, K. S. *J. Am. Chem. Soc.* **1991**, *113*, 6108−6110.
(10) Wang, B.; Wasielewski, M. R. *J. Am. Chem. Soc.* **1997**, *119*, 12−21.

10.1021/ic010827+ CCC: $22.00
Published on Web 02/14/2002

influence the MLCT luminescence energy and kinetics;[11] thus, coordination of analyte directly to the metal center can elicit a photophysical response.

Reversible analyte binding is desirable for continuous monitoring, so hemilabile ligands (bidentate ligands with one readily displaceable donor) may be used to achieve stable, coordinatively saturated complexes that are still able to act as an analyte receptor at the metal center.[12,13] In a recent paper,[14] we reported preliminary studies on $[Ru(bpy)_2(POMe\text{-}P,O)]^{2+}$ (**1**) (POMe = (2-methoxyphenyl)diphenylphosphine), a hemilabile ligand complex that responds to the binding of analytes such as acetonitrile, DMSO, and thiols via changes in both the absorption and low-temperature (77 K) emission spectra. These spectral changes are induced by the alteration of the ligand environment about the Ru(II) center. To our knowledge, this is the first example of an MLCT-based sensor designed to take advantage of the reversible binding provided by a hemilabile ligand. In this paper, we report our findings that water causes a dramatic concentration-dependent red shift of both the absorption and emission spectra of **1**. A related complex, $[Ru(bpy)_2(PO^iPr\text{-}P)(OH_2)](PF_6)_2$ (**2b**), is also reported, along with absorption and emission data.

Experimental Section

General Details. Chemicals were used as received unless otherwise specified. $Ru(bpy)_2Cl_2\cdot 2H_2O$[15] was prepared as described in the literature. $[Ru(bpy)_2(POMe\text{-}P,O)](PF_6)_2$, **1**, was available from previous studies.[14] Samples for NMR experiments were prepared at the concentrations specified in the text. Deuterated solvents were used as received from Cambridge Isotope Laboratories; anhydrous CD_2Cl_2 was prepared via distillation from P_2O_5 and stored in a N_2-filled drybox. NMR spectra were acquired on Bruker AC-200, Avance 300, and Avance 400 instruments, using residual solvent peaks as internal ^1H reference (vs TMS at δ 0) and 85% H_3PO_4 as external ^{31}P reference (δ 0). For the photophysical studies, anhydrous ethanol and HPLC grade acetone were either used as received or alternatively dried by treatment with a suitable drying agent (CaH_2 for ethanol, Drierite for acetone) followed by distillation. CH_2Cl_2 was distilled from CaH_2 immediately prior to use.

(2-(2-Propoxy)phenyl)diphenylphosphine (PO^iPr). This compound was prepared via a modification of the literature method.[16] 2-Lithio(2-propoxy)benzene was prepared by the reaction of *n*-BuLi (−78 °C/dry hexanes/N_2) with 2-(2-propoxy)bromobenzene.[17] Subsequent reaction with $ClPPh_2$ according to the literature method provided the desired phosphine in yield (~70%) similar to that previously reported.

Reaction of PO^iPr with $Ru(bpy)_2Cl_2\cdot 2H_2O$. A suspension of $Ru(bpy)_2Cl_2\cdot 2H_2O$ (0.670 g, 1.29 mmol) in nitrogen-sparged acetone (50 mL) was treated with $AgBF_4$ (0.506 g, 2.60 mmol) in acetone (20 mL). The mixture was thoroughly sparged with nitrogen, stirred at room temperature overnight to ensure complete precipitation of AgCl, and then filtered through Celite to yield a deep wine-red solution of the solvate complex. To this solution was added 1 equiv of (2-(2-propoxy)phenyl)diphenylphosphine (0.414 g, 1.29 mmol) as a solution in nitrogen-sparged acetone (5 mL), and the mixture was heated to reflux under nitrogen for 2 d to yield a red-orange solution. The cooled reaction mixture was filtered and evaporated to dryness and the residue dissolved in a small volume of acetone and precipitated with aqueous NH_4PF_6. The flocculent orange solid was collected, washed with water, dried by suction, and stored in a desiccator. Yield: 1.17 g. The composition of the isolated material is discussed in the Results and Discussion. A single crystal suitable for X-ray crystallographic analysis picked from material crystallized by slow evaporation of a solution in CH_2Cl_2/hexanes was determined to be the aquo complex **2b**.

Crystallographic Structure Determination of 2b. A single crystal of **2b** grown from CH_2Cl_2/hexanes was mounted onto a thin glass fiber. Measurements were made at 173(1) K on a Rigaku/ADSC CCD area detector using graphite-monochromated Mo Kα radiation. Data were collected in two sets of scans ($\phi = 0.0-190.0°$, $\chi = -90.0°$ and $\omega = -19.0°$ to $+23.0°$, $\chi = -90.0°$) using 0.50° oscillations with 12.0 s exposures. Data were collected and processed using the d*TREK program (Molecular Structure Corp.); the structure was solved using direct methods[18] and expanded using Fourier techniques.[19] The non-hydrogen atoms were refined anisotropically. One disordered molecule of CH_2Cl_2 was found to crystallize in the asymmetric unit. One PF_6^- anion displayed considerable thermal motion, which was modeled successfully as two separate fragments, with relative populations of 0.65 and 0.35, respectively. In addition, the isopropyl group [C(8)−C(7)−C(9)] was also found to be disordered and was modeled as two separate fragments, with relative populations of 0.57 and 0.43, respectively. Hydrogen atoms were included but not refined. All calculations were performed using the teXsan crystallographic software package (Molecular Structure Corp.). Crystallographic data for **2b** are summarized in Table 1 and selected interatomic distances and angles are listed in Table 2, and an ORTEP representation of the solid-state molecular structure prepared using ORTEP-3 for Windows[20] is depicted in Figure 1.

$^{31}P\{^1H\}$ NMR Spectroscopic Studies. Because low metal complex concentrations were required to observe the aquo complex **1b**, $^{31}P\{^1H\}$ NMR spectra were averaged over a large number of scans (NS > 1000). Experiments were performed using inverse-gated ^1H decoupling (i.e., decoupler on only during FID acquisition) to minimize $^1H-^{31}P$ NOE effects. To overcome the problems introduced by long and inequivalent ^{31}P longitudinal relaxation times (T_1), the paramagnetic complex $Cr(acac)_3$ was added to the solutions to shorten the relaxation times.[21] In the presence of $Cr(acac)_3$ (~2.5×10^{-2} M), spectra acquired using a delay of 2 s yielded integrals indistinguishable from those obtained from spectra acquired with a long delay (D1 = 20 s); a short acquisition time (AQ = 1 s) was sufficient to achieve complete decay of the magnetization. Using these parameters (inverse-gated decoupling, D1 = 2 s, AQ = 1 s),

(11) Caspar, J. V.; Meyer, T. J. *Inorg. Chem.* **1983**, *22*, 2444−2453.
(12) Bader, A.; Lindner, E. *Coord. Chem. Rev.* **1991**, *108*, 27−110.
(13) Slone, C. S.; Weinberger, D. A.; Mirkin, C. A. *Prog. Inorg. Chem.* **1999**, *48*, 233−350.
(14) Rogers, C. W.; Wolf, M. O. *Chem. Commun.* **1999**, 2297−2298.
(15) Lay, P. A.; Sargeson, A. M.; Taube, H. In *Inorganic Syntheses*; Lay, P. A., Sargeson, A. M., Taube, H., Eds.; John Wiley & Sons: Toronto, 1986; Vol. 24, pp 292−293.
(16) Horner, L.; Simons, G. *Phosphorus Sulfur* **1983**, *14*, 189−209.
(17) Aroyan, A. A. *Izv. Akad. Nauk. Arm. SSR., Khim. Nauki* **1964**, *17*, 532−542.
(18) Altomare, A.; Burla, M. C.; Cammalli, G.; Cascarano, M.; Giacovazzo, C.; Guagliardi, A.; Moliterni, A. G. G.; Polidori, G.; Spagna, A. *J. Appl. Crystallogr.* **1999**, *32*, 115−119.
(19) Beurskens, P. T.; Admiraal, G.; Beurskens, G.; Bosman, W. P.; deGelder, R.; Israel, R.; Smits, J. M. M. *The DIRDIF-94 program system*; Technical Report of the Crystallography Laboratory; University of Nijmegen: Nijmegen, The Netherlands, 1994.
(20) Farrugia, L. J. *J. Appl. Crystallogr.* **1997**, *30*, 565.
(21) Kasler, F.; Tierney, M. *Anal. Chem.* **1979**, *51*, 1070−1074.

Table 1. Summary of Crystallographic Data for **2b**

	$[Ru(PO^iPr\text{-}P)(OH_2)]^{2+}$, **2b**·$CH_2Cl_2$		$[Ru(PO^iPr\text{-}P)(OH_2)]^{2+}$, **2b**·$CH_2\mathbf{Cl_2}$
empirical formula	$C_{42}H_{41}Cl_2F_{12}N_4O_2P_3Ru$	V (Å^3)	2273.8(3)
fw	1126.69	Z	2
color, habit	red, block	ρ_{calcd} (g cm^{-3})	1.646
cryst size (mm)	0.35 × 0.20 × 0.15	μ(Mo Kα) (cm^{-1})	6.6
cryst syst	triclinic	temp (K)	173(1)
space group	$P\bar{1}$ (No. 2)	total no. of reflns	19508
a (Å)	12.5278(8)	no. of unique reflns	8682
b (Å)	13.554(2)	no. of obsd reflns[a]	6848
c (Å)	14.1049(8)	R1[b]	0.071
α (deg)	77.313(3)	wR2[c]	0.117
β (deg)	76.841(2)	GOF	1.45
γ (deg)	89.064(4)		

[a] $I > 3\sigma(I)$. [b] $R1 = \sum||F_o| - |F_c||/\sum|F_o|$ (observed data). [c] $wR2 = (\sum(F_o^2 - F_c^2)^2/\sum w(F_o^2)^2)^{1/2}$ (all data).

Table 2. Selected Interatomic Distances and Bond Angles for **2b**

Distances (Å)			
Ru(1)−O(2)	2.138(2)	Ru(1)−P(1)	2.3401(8)
Ru(1)−N(1)	2.096(3)	Ru(1)−N(2)	2.115(3)
Ru(1)−N(3)	2.032(3)	Ru(1)−N(4)	2.060(3)
F(8a)[a]−H(40)	2.12(6)	F(12b)[a]−H(40)	2.24(6)
O(1)−H(41)	2.07(5)		

Angles (deg)			
P(1)−Ru(1)−O(2)	90.06(7)	P(1)−Ru(1)−N(1)	99.10(8)
P(1)−Ru(1)−N(3)	95.40(8)	P(1)−Ru(1)−N(4)	90.67(8)
O(2)−Ru(1)−N(1)	95.3(1)	O(2)−Ru(1)−N(2)	83.7(1)
O(2)−Ru(1)−N(4)	91.0(1)	N(1)−Ru(1)−N(2)	78.0(1)
N(1)−Ru(1)−N(3)	93.2(1)	N(2)−Ru(1)−N(3)	91.3(1)

[a] F(8a) and F(12b) are part of a disordered PF_6 group.

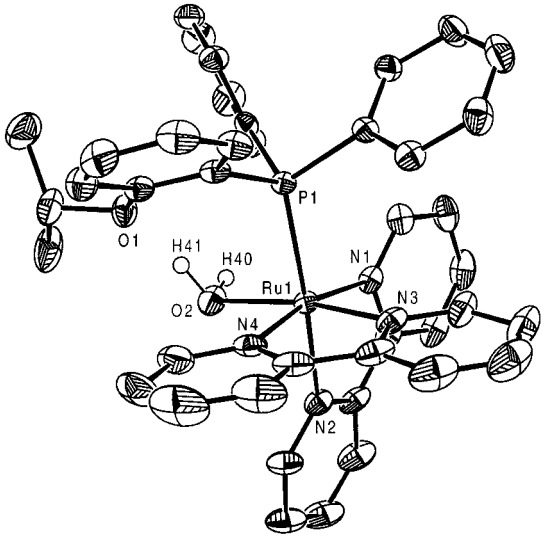

Figure 1. ORTEP representation of the solid-state molecular structure of **2b**. Hydrogen atoms and PF_6^- counterions are omitted for clarity; H(40) and H(41) were located but not refined.

$^{31}P\{^1H\}$ NMR experiments for samples containing mixtures of **1b** and **1** ($[\mathbf{1}]_i \approx 3 \times 10^{-3}$ M, $[H_2O] \approx 0.4-6$ M) required 1.5−3 h to achieve spectra with satisfactory signal-to-noise ratios.

The mixture of isopropyl derivatives was probed by $^{31}P\{^1H\}$ NMR spectroscopy in the absence of $Cr(acac)_3$ using short delay times and full ^1H decoupling. Thus, the uncertainty in the $^{31}P\{^1H\}$ NMR spectral integrations prevents accurate quantitation of the ratios of **2a**−**c**; however, the results are qualitatively useful.

Photophysical Studies. Room-temperature UV/vis absorption measurements were performed using a Unicam UV series 2 or Perkin-Elmer Lambda 2S spectrophotometer. Luminescence spectra were measured on an SLM 48000S fluorometer equipped with a sample holder cooled to 77 K. Emission lifetime measurements were carried out in an Oxford Instruments liquid-nitrogen-cooled cryostat. A pulsed Laser Photonics nitrogen laser was used as excitation source (337 nm). The samples were frozen−pumped−thawed−degassed for 4−5 cycles. Time-resolved emission was collected through a one-stage monochromator 90° from the incident excitation beam. The data were collected from a Hamamatsu R4220P photomultiplier tube on a Tektronix TDS544A transient digitizer. Lifetime data were fitted to exponential decays using a nonlinear least-squares fitting routine available in Microcal Origin 6.0.

Results and Discussion

Synthesis and Characterization. $[Ru(bpy)_2(POMe\text{-}P,O)](PF_6)_2$ (**1**) contains a *P*,*O*-bound phosphine−ether ligand and is easily prepared in pure form via the reaction of the phosphine−ether with the solvate complex $[Ru(bpy)_2(O{=}C(CH_3)_2)_2](BF_4)_2$ followed by metathesis to the hexafluorophosphate salt.[14] Using the analogous phosphine−isopropyl ether (PO^iPr), however, this synthetic procedure gives a mixture comprised of three major products, as determined by $^{31}P\{^1H\}$ NMR spectroscopy. In CD_2Cl_2 solution, the spectrum contained singlets at δ 50.7, 40.9, and 36.9 in a ∼7:5:1 ratio. The spectrum also contained a minor peak at δ 29.9 and a septet at δ −144 due to the PF_6^- anion. The singlet at δ 50.7 was tentatively assigned as $[Ru(bpy)_2(PO^i\text{-}Pr\text{-}P,O)](PF_6)_2$ (**2a**) on the basis of the similarity to the chemical shift of **1** (δ 52.8). The other two major components were assigned by addition of water and acetone to the NMR samples, which resulted in changes in the spectra. Addition of water caused an increase in the signal at δ 40.9, which suggests that this resonance is due to the complex $[Ru(bpy)_2(PO^iPr\text{-}P)(OH_2)](PF_6)_2$ (**2b**) in which water is coordinated. Addition of acetone resulted in an increase in the resonance at δ 36.9, which could then be the analogous acetone complex $[Ru(bpy)_2(PO^iPr\text{-}P)(O{=}C(CH_3)_2)](PF_6)_2$ (**2c**). Both of these experiments also resulted in a decrease in the signal at δ 50.7.

Attempts were made to remove water and acetone from the mixture to obtain pure **2a**. Heating the solid in vacuo over P_2O_5 at 60 °C for 3 weeks resulted in only a slight

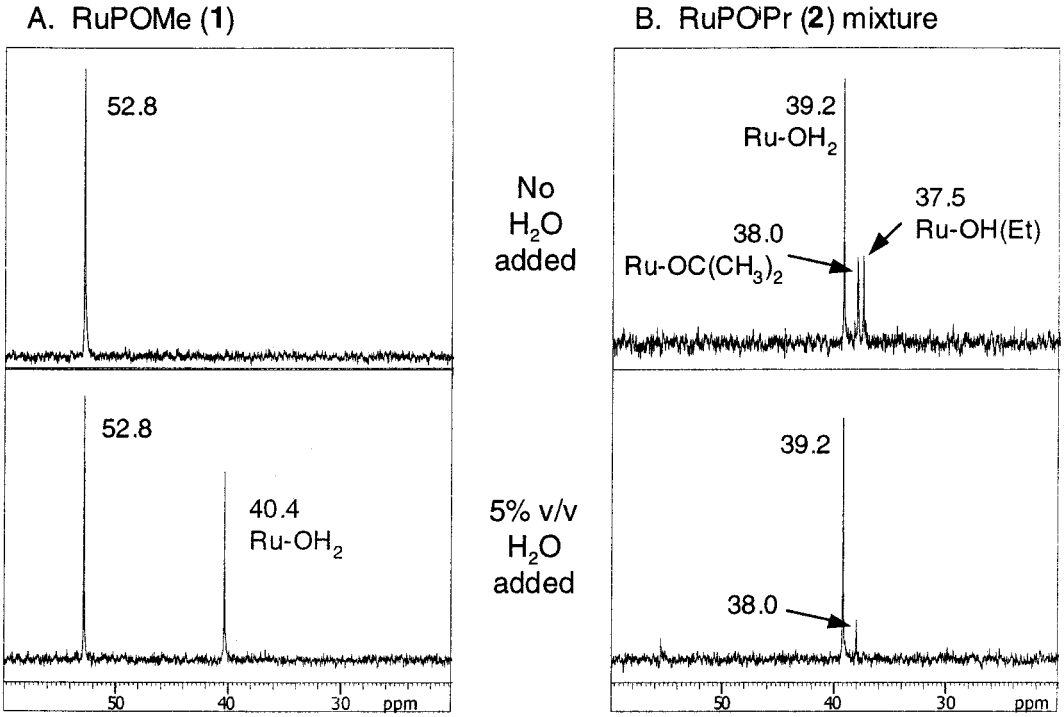

Figure 2. $^{31}P\{^1H\}$ NMR spectra for **1** and **2** in 2:1 ethanol/acetone-d_6 solution (10^{-3} M in Ru), before and after addition of 5% (v/v) water.

improvement in the relative amount of **2a** present. Heating the solid to higher temperatures to drive off water and acetone resulted in gradual decomposition. Crystallization and chromatographic techniques also did not effect bulk separation of the three complexes. Modified synthetic routes using anhydrous $Ru(bpy)_2Cl_2$ as a starting material and employing rigorously dried solvents (acetone, THF) were also unsuccessful. Attempts to use $Ru(bpy)_2(OTf)_2$ as a starting material led to very sluggish reactions and did not give the desired products.

Structural Determination of 2b. Crystallization of the complex mixture via slow evaporation of a solution in CH_2Cl_2/hexanes, though not useful for the bulk separation of the complexes, did give some high-quality crystals. A single crystal picked from the crystallized mixture was structurally characterized by X-ray crystallographic analysis and determined to be the aquo complex **2b**. The crystallographic data are summarized in Table 1, and selected interatomic distances and bond angles are listed in Table 2. An ORTEP representation of the solid-state molecular structure is depicted in Figure 1. The geometry about the Ru(II) center is distorted octahedral with one of the coordination sites occupied by a water molecule. The coordinated water molecule is engaged in intramolecular hydrogen bonding, with interactions present both between H(41) and the isopropyl ether oxygen atom and between H(40) and the fluorines of the disordered hexafluorophosphate anions that are not shown in Figure 1. The Ru−O distance (2.138(2) Å) is similar to that found in other ruthenium(II) aquo complexes (Ru−O = 2.122(16) Å in $[Ru(OH_2)_6]^{2+}$,[22] Ru−O = 2.15 Å in $[RuH(OH_2)(CO)_2(PPh_3)_2]^+$[23]). The Ru−N bond lengths are typical of those observed in related dicationic ruthenium(II) bipyridyl phosphine−ether complexes,[24] including complex **1**. The Ru−P distance (2.3401(8) Å) is significantly longer than in these related phosphine−ether complexes (Ru−P = 2.2908(6) Å in **1**), but is similar to that observed in an analogous $[Ru(bpy)_2(POR\text{-}P)L]^{2+}$ complex (R = CF_3, L = CH_3CN; Ru−P = 2.3561(8) Å).[25]

NMR Studies. The low-temperature photophysical studies described later in this paper were carried out at 77 K in frozen 2:1 ethanol/acetone solution. We were therefore interested in examining NMR spectra of these complexes in this solvent mixture and at the same concentrations used in the photophysical studies to determine whether any chemical changes due to these conditions may be observed. At the concentration typically used for NMR experiments ($\sim 10^{-2}$ M), solutions of **1** in CD_2Cl_2, acetone-d_6, and 2:1 ethanol/acetone-d_6 all show one sharp singlet in the $^{31}P\{^1H\}$ NMR spectrum near δ 50, assigned to the *P*,*O*-bound complex. NOE experiments verify that this peak corresponds to the *P*,*O*-coordinated complex since an NOE is observed between the methyl group and a proton on one of the bipyridyl rings. Addition of water to these solutions has no effect on the spectrum. However, at 10^{-3} M in 2:1 ethanol/acetone, addition of 5% (v/v) H_2O results in the appearance of a ^{31}P resonance at δ 40.4 assigned to a new compound, **1b**, significantly upfield of the signal at δ 52.8 due to **1** (Figure 2). On the basis of this behavior, and the isolation of the aquo complex **2b**, we assign **1b** as the aquo complex. There

(22) Bernhard, P.; Burgi, H.-B.; Hauser, J.; Lehmann, H.; Ludi, A. *Inorg. Chem.* **1982**, *21*, 3936−3941.

(23) Boniface, S. M.; Clark, G. R.; Collins, T. J.; Roper, W. R. *J. Organomet. Chem.* **1981**, *206*, 109−117.

(24) Rogers, C. W.; Wolf, M. O. *J. Chem. Soc., Dalton Trans.* **2001**, 1278−1283.

(25) Rogers, C. W.; Wolf, M. O. Unpublished results.

Scheme 1

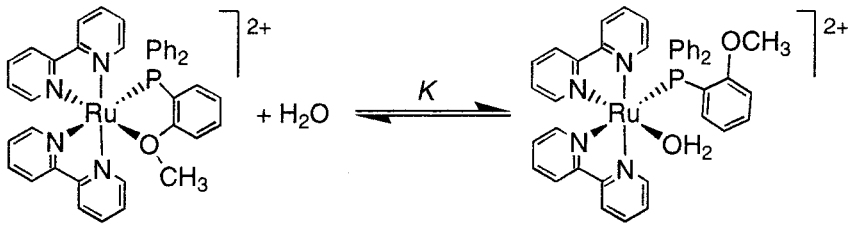

1 **1b**

is no evidence for the formation of an acetone complex in the $^{31}P\{^{1}H\}$ NMR spectrum in this case.

Complexes **1** and **1b** exist in equilibrium in the presence of water, as depicted in Scheme 1. Two mechanisms are possible for the reaction of **1** with water:

(a) a concerted interchange mechanism in which the ether competes with water for the labile coordination site, and the reaction proceeds via a 7-coordinate transition state, or

(b) a stepwise dissociative−associative mechanism in which the ether and water compete for binding to a 5-coordinate intermediate.

Both mechanisms require consideration of the effective concentration of the displaced ether moiety, and lead to an equilibrium expression of the form

$$K = \frac{[\mathbf{1b}](\alpha[\text{“OMe”}])}{[\mathbf{1}][H_2O]}$$

where the concentration of displaced ether [“OMe”] = [**1b**] because the ether is a component of the aquo complex. The proportionality constant α accounts for the fact that the ether is tethered in close proximity to the metal center and therefore has a higher effective concentration than it would have if it were free in solution. Thus, the equilibrium expression becomes

$$K_{\text{eff}} = \frac{K}{\alpha} = \frac{[\mathbf{1b}]^2}{[\mathbf{1}][H_2O]}$$

and a plot of $[\mathbf{1b}]^2/[\mathbf{1}]$ vs $[H_2O]$ should be linear. Indeed, the ratio of aquo complex to *P*,*O*-complex determined by monitoring a titration of **1** with H_2O via $^{31}P\{^{1}H\}$ NMR spectroscopy was found to scale nonlinearly with $[H_2O]$. As shown in Figure 3, a linear relationship is observed for the data when $[\mathbf{1b}]^2/[\mathbf{1}]$ is plotted vs $[H_2O]$. It should be noted that the true equilibrium constant *K* cannot be determined without knowledge of the effective ether concentration, which requires determination of the proportionality constant α. The equilibrium constants originally reported for reaction of **1** with other analytes[14] using a simpler equilibrium expression have been recalculated using the equilibrium given here.[26]

The data shown in Figure 3 yield an effective equilibrium constant for the reaction of **1** with water of $K_{\text{eff}} = (6 \pm 3) \times 10^{-3}$. The reversibility of the reaction was confirmed by reestablishment of equilibrium after addition of more **1** to the mixture. It should be emphasized that, with such a small

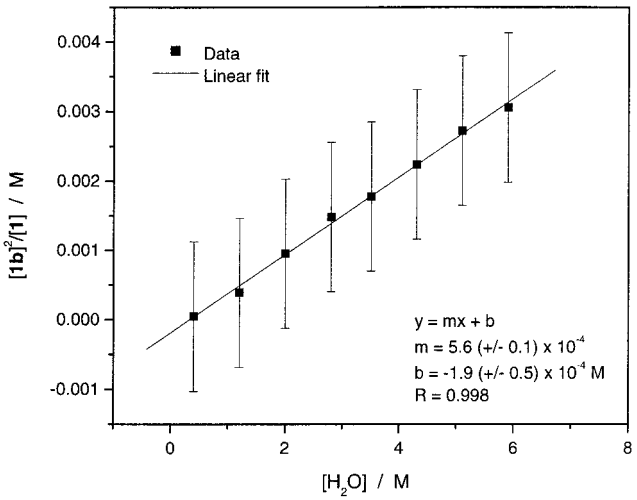

Figure 3. $[\mathbf{1b}]^2/[\mathbf{1}]$ vs $[H_2O]$ as determined from integration of $^{31}P\{^{1}H\}$ NMR spectra of **1** in 2:1 ethanol/acetone-d_6 solution, $[\mathbf{1}] = 3.3 \times 10^{-3}$ M, with increasing water content. Error bars are $\pm 1\sigma$ from the data.

formation constant, the aquo complex **1b** is observable by NMR spectroscopy only when the concentration of water is quite large (>0.2 M) and the total metal concentration is relatively low. This situation arises as described above by deliberately adding water to a sample. Residual water contained in commercially available organic solvents (~0.5% v/v ≈ 0.3 M H_2O) is insufficient to produce an amount of aquo complex detectable by $^{31}P\{^{1}H\}$ NMR spectroscopy.

The $^{31}P\{^{1}H\}$ NMR spectrum of the isopropyl ether complex mixture **2** is solvent dependent. At 10^{-2} M in CD_2Cl_2, resonances corresponding to the *P*,*O*-complex **2a**, aquo complex **2b**, and acetone complex **2c** are all present. As expected, in acetone-d_6 the resonance due to **2a** is greatly diminished due to formation of the acetone complex **2c** (Scheme 2). At 10^{-3} M in 2:1 ethanol/acetone-d_6 solution, *P*,*O*-complex **2a** is absent; the resonances due to the aquo complex **2b** (δ 39.2) and acetone complex **2c** (δ 38.0) are present, as is an additional resonance (δ 37.5), possibly due to an ethanol complex (**2d)** (Figure 2). Upon addition of 5% (v/v) H_2O, the resonance at δ 37.5 disappears and the intensity of the resonance due to the aquo complex **2b** increases relative to that of the acetone complex **2c**.

Photophysical Studies. Absorption spectra at 298 K and emission spectra at 77 K of complex **1** in 2:1 ethanol/acetone

(26) Analyte (K_{eff}): MeCN (>360); Me_2S (1.7 ± 0.3); EtSH (0.11 ± 0.02); $C_{12}H_{14}SH$ (0.12 ± 0.03); DMSO (0.015 ± 0.002 and 0.0006 ± 0.0001, pseudoequilibrium constants calculated as if the two species are independent of each other).

Scheme 2

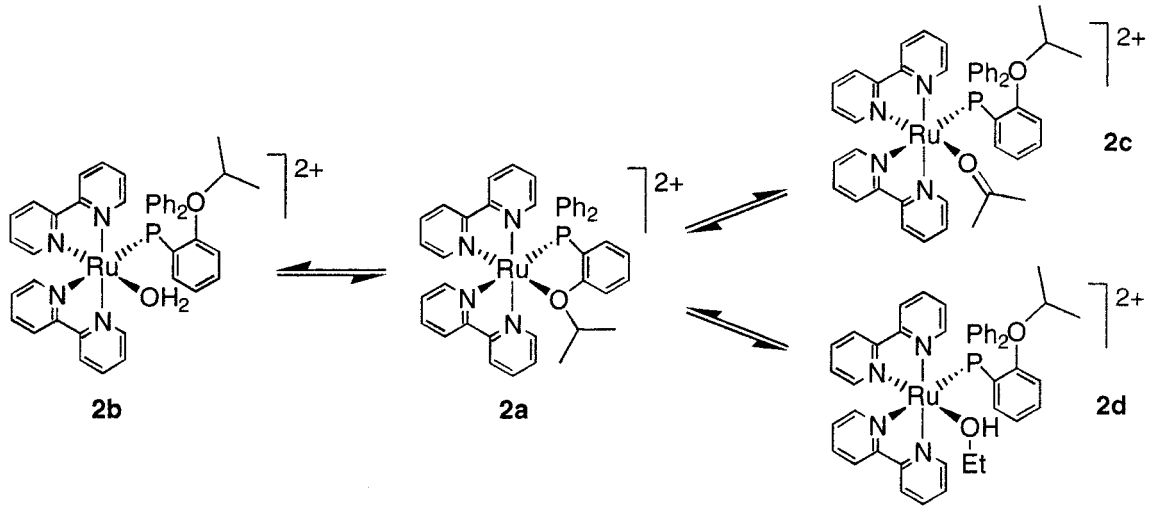

solution were determined over a range of concentrations (10^{-3} to 10^{-5} M). Two sets of bands were observed in the absorption spectra for complex **1**. The lower energy bands (λ_{max} = 414 nm at high concentration and 448 nm at low concentration) responsible for the orange color can be assigned to spin-allowed dπ(Ru) → π^*(ligand) MLCT absorptions by analogy to other ruthenium bis(bipyridyl) complexes.[3,4,11] The intensity of the MLCT absorption (ϵ = 6700 M^{-1} cm^{-1} at the high-concentration limit) is lower than for $[Ru(bpy)_3]^{2+}$ (λ_{max} = 452 nm, ϵ = 14454 M^{-1} cm^{-1})[27] because there are fewer bipyridine ligands in **1**. The higher energy bands (around 300 nm) can be assigned to bipyridyl-based $\pi \rightarrow \pi^*$ transitions of the aromatic ligands.

The emission spectrum in concentrated solution (10^{-3} M) consists of a broad, slightly structured band centered at approximately 600 nm with a long tail to lower energy. The highest energy emission band (λ_{em} = 542 nm, E_{em} = 18.5 × 10^3 cm^{-1}) is considerably weaker in intensity than the band with λ_{em} = 588 nm (E_{em} = 17.0 × 10^3 cm^{-1}), which dominates the spectrum and accounts for the red-orange color of the emission. Emission spectra for $[Ru(bpy)_2L_2]^{2+}$ complexes typically show a gradual decrease in band intensity with decreasing energy across the vibrational progression, and a pronounced low-energy tail.[11] The vibrational progression is generally attributed to vibrations within the bipyridine ligand framework. Thus, the diminutive highest energy band observed for **1** is unusual; this transition might be disfavored due to geometrical constraints imposed by the five-membered *P*,*O*-chelate ring. It is unlikely to be related to symmetry considerations since a complex containing a different asymmetric chelate with *N*,*N*′-coordinated 2-(2-aminoethyl)-pyridine[4] shows the typical vibrational progression in its emission spectrum.

Both the MLCT absorption band and the emission spectrum become red-shifted as the concentration of **1** decreases, as shown in Figure 4. The onset of the spectral red shift occurs at the same concentration, approximately 1 × 10^{-4} M, for both absorption and emission, and the shift

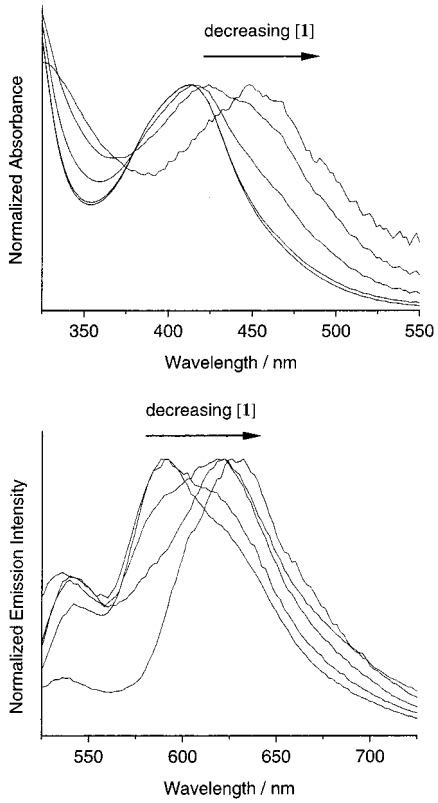

Figure 4. Concentration-dependent absorption (room temperature) and photoluminescence (77 K) spectra for **1** in 2:1 ethanol/acetone solution containing residual water (~0.3 M). From left to right, [**1**] = 1 × 10^{-3}, 5 × 10^{-4}, 2 × 10^{-4}, 1 × 10^{-4}, and 3 × 10^{-5} M.

is complete by 10^{-5} M. At the high-concentration limit (10^{-3} M), complex **1** shows a maximum absorption at 414 nm and maximum emission at 588 nm, whereas at the low-concentration limit (10^{-5} M), maximum absorption occurs at 448 nm and maximum emission occurs at 629 nm. The two absorption bands are of similar intensity (ϵ_{414} = 6700 ± 100 M^{-1} cm^{-1}, ϵ_{448} = 8000 ± 600 M^{-1} cm^{-1}); however, the lower energy MLCT band observed for low concentrations of **1** is broadened slightly relative to the band observed at high concentration. Figure 4 shows the dramatic 30−40 nm red shift of both the absorption and emission spectra that

(27) Crutchley, R. J.; Lever, A. B. P. *Inorg. Chem.* **1982**, *21*, 2276−2282.

occurs when the concentration of **1** is decreased from 10^{-3} to 10^{-5} M. This effect is unusual for two reasons: first, ruthenium(II) bipyridyl complexes do not typically show concentration-dependent absorption or emission spectra, and second, we have not encountered any evidence for dimerization or other intermolecular interactions in our studies of complex **1**.

Given that NMR spectroscopic experiments have shown that complex **1** is in equilibrium with an aquo complex in "wet" solvents, this concentration dependence can be explained on the basis of the presence of adventitious water in the solvent. Indeed, the magnitude of the absorption spectral red shift at low concentrations depends on how dry the solvents are. Solutions prepared in anhydrous CH_2Cl_2 (λ_{max} = 413 nm) do not show this concentration-dependent red shift, nor do those prepared in CH_2Cl_2 to which some water has been added, presumably due to the low miscibility of water with CH_2Cl_2. Low-concentration solutions in ethanol/acetone (10^{-5} M) show larger red shifts when prepared using commercial solvents as received from the suppliers (~0.3 M H_2O) than when prepared using solvents rigorously dried using accepted protocols. Addition of 5% (v/v) water (~3 M) to concentrated solutions of **1** in 2:1 ethanol/acetone ([**1**] = 10^{-3} M) results in a noticeable red shift and broadening of the MLCT band; the absorption maximum shifts from 411 to 419 nm. This treatment corresponds to an increase in the relative [H_2O]:[**1**] ratio from approximately 1000:1 to 10000:1, and the observed shift in the absorption spectrum is consistent with the small equilibrium constant (K_{eff} = (6 ± 3) × 10^{-4}) determined from the NMR spectroscopic data. For a sample containing 10^{-3} M **1**, an increase from 0.3 to 3 M water should result in a change in the [**1b**]:[**1**] ratio from ~1.0:1.9 to 2.5:1.0, which is a large enough change in speciation to produce noticeable spectral changes for two species with significantly different MLCT transition energies.

Efforts to confirm the presence of **1b** in dilute solution (4 × 10^{-4} and 4 × 10^{-5} M in Ru) in the absence and presence of added water were unsuccessful due to the insufficient signal-to-noise ratios obtained even after overnight acquisitions of the $^{31}P\{^1H\}$ NMR spectra. When K_{eff} is considered, the low-concentration limit (3 × 10^{-5} M in Ru, ~0.3 M in H_2O) emission spectrum corresponds to a mixture of **1b** and **1** in a ratio of approximately 6.9:1.0. Thus, at low metal concentrations in the absence of added water, the predominant species is the aquo complex **1b**, while at high metal concentrations the observed spectra arise predominantly from **1**.

The isopropyl derivative **2** shows similar absorption behavior. In CH_2Cl_2 solution, spectra of **2** measured at high and low concentrations are essentially superimposable (λ_{max} = 419−420 nm). In dry 2:1 ethanol/acetone solution, low-concentration samples (10^{-5} M, λ_{max} = 454 nm) show red-shifted spectra relative to high-concentration samples (10^{-3} M, λ_{max} = 434 nm). Here, the high-concentration limit absorption band is consistently at lower energy than for complex **1** because, even in anhydrous solvents, **2** contains *P*,*O*-complex **2a**, aquo complex **2b**, acetone complex **2c**, and ethanol complex **2d**. The addition of 5% (v/v) water to these solutions has a negligible effect on the spectra, likely due to the complex equilibria involving acetone, ethanol, and water in competition for reaction with the *P*,*O*-coordinated complex.

The altered coordination sphere in **1b** compared to **1** must account for the observed differences in photophysical properties. The MLCT transition was lowered in energy by ~0.23 eV (18.3 × 10^3 cm^{-1}) according to the absorption spectrum (34 nm red shift). The emission maximum from the MLCT excited state was also lowered in energy, but by a larger amount (0.32 eV = 25.5 × 10^3 cm^{-1}), as determined from the 87 nm red shift. It is noteworthy that there is very little red shift in the emission energy of the first observable band in the vibrational progression (Figure 4). The decreased MLCT energy signifies either stabilization of the bpy π^* acceptor orbitals or destabilization of the filled metal dπ donor orbital. It is difficult to see how the energetics of the bpy π^* orbitals would be strongly affected by coordination sphere changes since the faces of the bpy rings are rather distant from the labile site. On the other hand, simple replacement of an ether with a water molecule does not in itself seem likely to cause dramatic changes in electron density at the metal. Removal of the *P*,*O*-chelate ring strain upon displacement of the ether, however, may play an important role. Geometric constraints imposed by the *P*,*O*-chelate do appear to have a profound effect on the MLCT excited state, when one considers the change in the vibrational structure of the emission spectrum of **1**. Therefore, the dominant dπ orbital destabilization presumably arises from improved ligand−metal orbital overlaps and their effect on the electron density at the metal center.

Excited-state lifetimes for emission from **1** at 77 K in solid 2:1 ethanol/acetone solution containing residual water (~0.3 M) were determined for samples at both high- and low-concentration limits. The data were satisfactorily fit to a single-exponential decay, as shown in Figure 5, consistent with a unimolecular decay path. The first 50 ns of the decay was not included in the fit due to residual laser line scatter which occurred within the instrument response function. The emission lifetimes were found to be τ = 2.13 ± 0.02 and 1.95 ± 0.02 μs for the high- and low-concentration limits, respectively (Table 3). Both of these species, **1** and **1b**, have significantly shorter excited-state lifetimes at 77 K than $[Ru(bpy)_3]^{2+}$.[28]

Complexes of the type $Ru(bpy)_2L_2^{2+}$, where L is a phosphine ligand, are nonemissive at room temperature; however, emission can easily be observed at 77 K.[11] This temperature dependence is believed to be due to population of nonemissive metal-centered dd excited states that are thermally accessible from the MLCT state at room temperature. It is reasonable that, in the phosphine complexes studied here, the nonemissive behavior at room temperature is due to a similar reduction in the activation barrier between the MLCT and dd states. The phosphine complex $[Ru(bpy)_2(dmpe)]^{2+}$ (dmpe = 1,2-dimethylphosphinoethane) has a substantially longer lifetime than either **1** or **1b** at 77 K.[11]

(28) Watts, R. J.; Crosby, G. A. *J. Am. Chem. Soc.* **1972**, *94*, 2606−2614.

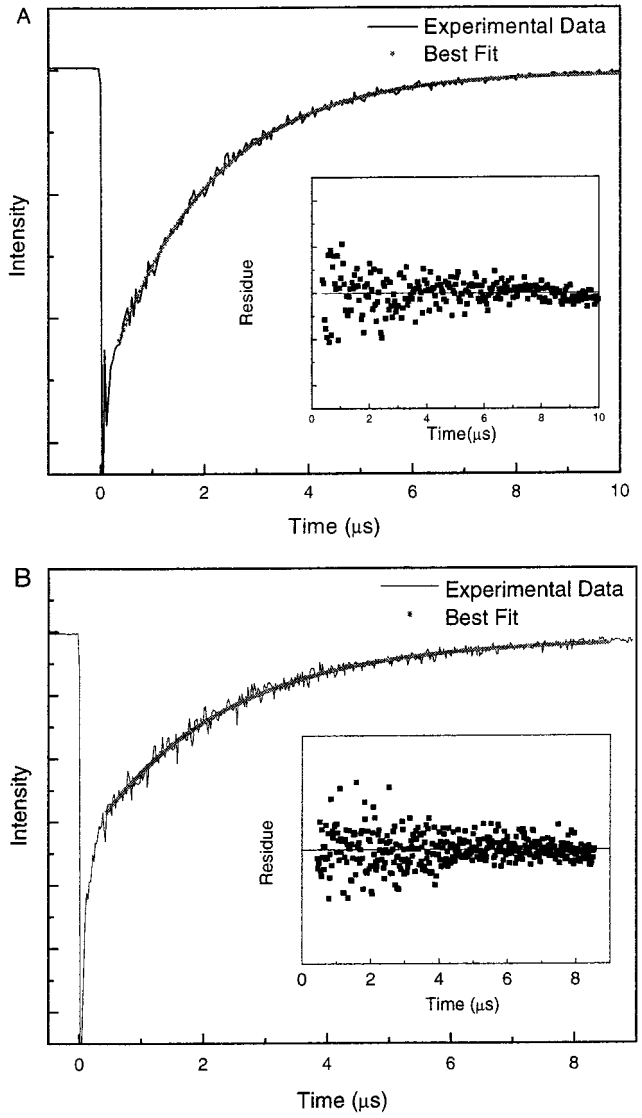

Figure 5. Emission decay traces for lifetime determination of **1** at 77 K in solid 2:1 ethanol/acetone solution containing residual water (~0.3 M). Panel A: [**1**] = 3×10^{-5} M, $\tau = 1.95 \pm 0.02$ μs. Panel B: [**1**] = 1×10^{-3} M, $\tau = 2.04 \pm 0.07$ μs. The insets show residuals plots (data are from the first-order decay model).

This suggests that even at low temperature other deactivation pathways are accessible for these phosphine−ether complexes. The hemilabile nature of the phosphine ligand is expected to provide additional nonradiative decay paths even in a solvent glass, consistent with the shorter lifetimes observed here.

Table 3. Photophysical Data for Phosphine−Ether and Related Ruthenium Bipyridyl Complexes[a]

complex	λ_{abs}/nm[b]	ϵ/M^{-1} cm^{-1} [b]	λ_{em}/nm[c]	τ_{em}/μs[c]
1				
1×10^{-3} M	414	6700 ± 100	588	2.13 ± 0.02
3×10^{-5} M	448	8000 ± 600	629	1.95 ± 0.02
2 (mixture)				
1×10^{-3} M	434	~6400	ND[h]	ND
3×10^{-5} M	454	~6600	ND	ND
$[Ru(bpy)_3]^{2+}$	443[d]	14454	584[e,g]	5.21 ± 0.06[c,f,g]
$[Ru(bpy)_2(dmpe)]^{2+}$			557[e]	6.2[e,g]

[a] In 2:1 ethanol:acetone solution. [b] At room temperature. [c] At 77 K. [d] In aqueous solution. [e] Reference 11. [f] Reference 28. [g] In 4:1 ethanol/methanol glass. [h] ND = not determined.

Conclusions

1 shows concentration-dependent shifts in both room-temperature absorption and low-temperature (77 K) luminescence spectra due to its reversible reaction with residual water in the solvent to form an aquo complex. The dramatic spectral shifts in response to the presence of water make complex **1** and its derivatives attractive for further study as chemosensory materials. From a comparison of complexes **1** and **2**, it is clear that the reactivity of phosphine−ether complexes toward small molecules can be tuned by changing the ether substituent. The ^{i}Pr group makes the ether moiety more labile, as expected from steric considerations. As a result, the Me derivative **1** shows a clean photophysical response to low concentrations of water, while the chemistry of the ^{i}Pr derivative **2** is complicated by additional equilibria involving solvate complexes.

Acknowledgment. We thank the Natural Sciences and Engineering Research Council of Canada (NSERC) and the National Institutes of Health (NIH) (Grant No. 1R15ES10106-01) for support of this research. C.W.R. thanks the NSERC and the University of British Columbia for graduate fellowships.

Supporting Information Available: X-ray crystallographic data for **2b** in CIF format. This material is available free of charge via the Internet at http://pubs.acs.org.

IC010827+